Cyanide Binding to Truncated Hemoglobins: A Crystallographic and Kinetic Study[†,‡]

Mario Milani,[&] Yannick Ouellet,[§] Hugues Ouellet,[§] Michel Guertin,[§] Alberto Boffi,[⊥] Giovanni Antonini,[#,||] Alessio Bocedi,[#,||,$] Marco Mattu,[#,||] Martino Bolognesi,[%] and Paolo Ascenzi[*,#,||]

Istituto Giannina Gaslini, Largo G. Gaslini, 5. 16147 Genova, Italy, Departement de Biochimie et de Microbiologie, Pavillon Marchand, Université Laval, Faculté des Sciences et de Génie, Quebec G1K 7P4, Canada, CNR, Centro di Biologia Molecolare, Dipartimento di Scienze Biochimiche 'Alessandro Rossi Fanelli', Università di Roma 'La Sapienza', Piazzale Aldo Moro 5, I-00185 Roma, Italy, Dipartimento di Biologia, Università 'Roma Tre', Viale Guglielmo Marconi 446, I-00146 Roma, Italy, Laboratorio Interdipartimentale di Microscopia Elettronica, Università 'Roma Tre', Via della Vasca Navale 79, I-00146 Roma, Italy, Dipartimento di Chimica, Ingegneria Chimica e Materiali, Università di L'Aquila, Via Vetoio, Coppito, I-67100 L'Aquila, Italy, and Dipartimento di Fisica-INFM, Centro d'Eccellenza per la Ricerca Biomedica, and Istituto Nazionale Ricerca sul Cancro, Università di Genova, Via Dodecaneso 33, I-16146 Genova, Italy

Received January 16, 2004; Revised Manuscript Received February 26, 2004

ABSTRACT: Cyanide is one of the few diatomic ligands able to interact with the ferric and ferrous heme-Fe atom. Here, the X-ray crystal structure of the cyanide derivative of ferric *Mycobacterium tuberculosis* truncated hemoglobin-N (*M. tuberculosis* trHbN) has been determined at 2.0 Å (*R*-general = 17.8% and *R*-free = 23.5%), and analyzed in parallel with those of *M. tuberculosis* truncated hemoglobin-O (*M. tuberculosis* trHbO), *Chlamydomonas eugametos* truncated hemoglobin (*C. eugametos* trHb), and sperm whale myoglobin, generally taken as a molecular model. Cyanide binding to *M. tuberculosis* trHbN is stabilized directly by residue TyrB10(33), which may assist the deprotonation of the incoming ligand and the protonation of the outcoming cyanide. In *M. tuberculosis* trHbO and in *C. eugametos* trHb the ligand is stabilized by the distal pocket residues TyrCD1(36) and TrpG8(88), and by the TyrB10(20) − GlnE7-(41) − GlnE11(45) triad, respectively. Moreover, kinetics for cyanide binding to ferric *M. tuberculosis* trHbN and trHbO and *C. eugametos* trHb, for ligand dissociation from the ferrous trHbs, and for the reduction of the heme-Fe(III)-cyanide complex have been determined, at pH 7.0 and 20.0 °C. Despite the different heme distal site structures and ligand interactions, values of the rate constant for cyanide binding to ferric (non)vertebrate heme proteins are similar, being influenced mainly by the presence in the heme pocket of proton acceptor group(s), whose function is to assist the deprotonation of the incoming ligand (i.e., HCN). On the other hand, values of the rate constant for the reduction of the heme-Fe(III)-cyanide (non)vertebrate globins span over several orders of magnitude, reflecting the different ability of the heme proteins considered to give productive complex(es) with dithionite or its reducing species SO_2^-. Furthermore, values of the rate constant for ligand dissociation from heme-Fe(II)-cyanide (non)vertebrate heme proteins are very different, reflecting the different nature and geometry of the heme distal residue-(s) hydrogen-bonded to the heme-bound cyanide.

Cyanide is one of the few ligands that is able to interact with both ferric and ferrous heme-Fe atom, albeit with very different thermodynamic and kinetic parameters, representing a valuable diatomic ligand model system. Notably, cyanide is isosteric and isoelectronic with the diatomic carbon monoxide heme-Fe(II) ligand (*1*−*3*).

The complexes formed by cyanide with ferric heme proteins [e.g., hemoglobin (Hb) and myoglobin (Mb)][1] are very stable, values of the association equilibrium constant being higher than 10^5 M^{-1}. The different stability of heme-Fe(III)-cyanide complexes is primarily determined by the rate of ligand dissociation (the values of the first-order dissociation rate constant range between 1×10^{-2} and 1×10^{-6} s^{-1}). On the other hand, values of the second-order rate constant for cyanide binding to ferric Mbs and Hbs (i.e., k_{on})

[†] This study was supported by grants from the Italian Ministry for Education, University, and Research (FIRB Project RBAU015B47_002 to M.B.; 'Università Roma Tre − Fondi per lo Sviluppo 2003′ to P.A.), from the Italian National Research Council (Functional Genomics to M.B.), and from the Natural Sciences and Engineering Research Council of Canada 46306-01 grant to M.G. Moreover, M.B. is grateful to Istituto Giannina Gaslini (Genova, Italy) and to Fondazione Compagnia di San Paolo (Genova, Italy) for continuous support.

[‡] The atomic coordinates and structure factors for the cyanide derivative of ferric *M. tuberculosis* trHbN have been deposited within the Protein Data Bank (PDB entry: 1RTE), from which copies are available.

* To whom all correspondence should be addressed. Telephone: +39+06-5517-3200(2). Fax: +39+06-5517-6321. E-mail: ascenzi@uniroma3.it.

[&] Istituto Giannina Gaslini.

[§] Université Laval.

[⊥] Università di Roma 'La Sapienza'.

[#] Dipartimento di Biologia, Università 'Roma Tre'.

[||] Laboratorio Interdipartimentale di Microscopia Elettronica, Università 'Roma Tre'.

[$] Università di L'Aquila.

[%] Università di Genova.

[1] Abbreviations: Hb, hemoglobin; Mb, myoglobin; trHb, truncated hemoglobin; *A. limacina* Mb, *Aplysia limacina* monomeric Mb; *C. eugametos* trHb, *Chlamydomonas eugametos* monomeric trHb; *M. tuberculosis* trHbN, *Mycobacterium tuberculosis* homodimeric trHb (component N); *M. tuberculosis* trHbO, *Mycobacterium tuberculosis* homododecameric trHb (component O); *P. equorum* Hb, *Parascaris equorum* homooctameric Hb; rmsd, root-mean-squares deviation. Amino acid residues have been identified by their three-letter code, their topological position, and their sequence number within parentheses.

10.1021/bi049870+ CCC: $27.50
Published on Web 04/07/2004

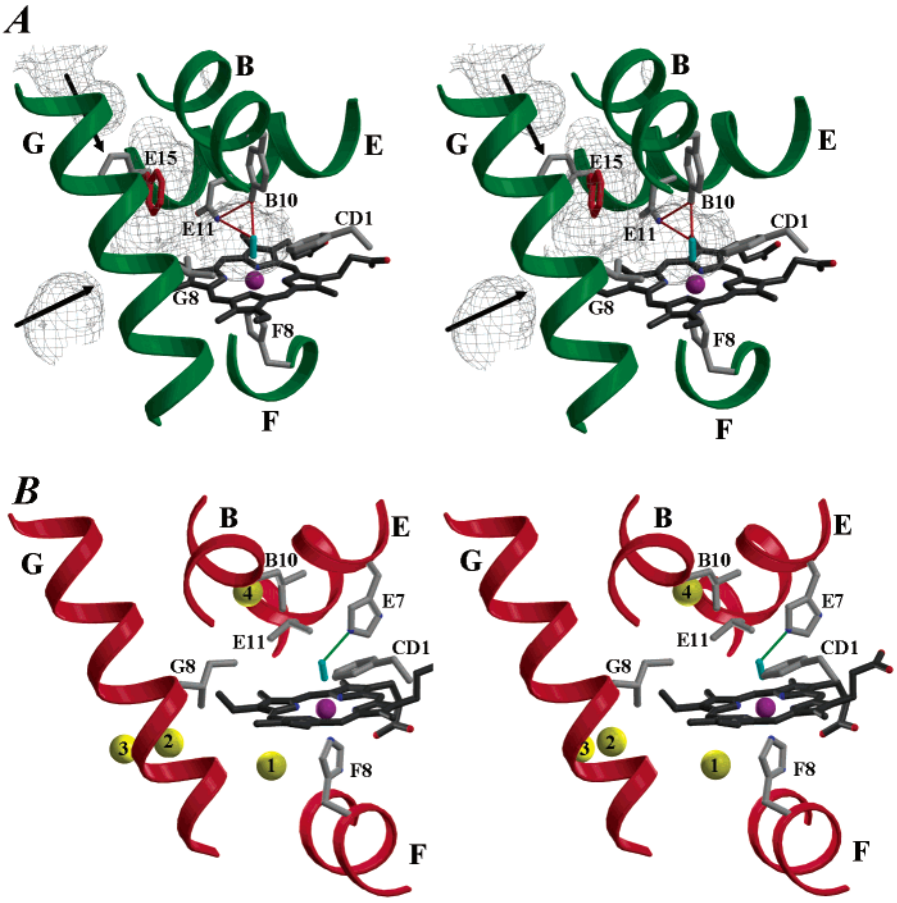

FIGURE 1: (A) Stereoview of the heme pocket region in cyano-met *M. tuberculosis* trHbN (PDB entry: 1RTE) (*24*), displaying part of the surrounding protein structure (green ribbons), the heme group (black), the cyanide ligand (cyan), and key residues (grey) stabilizing the heme-Fe-bound cyanide. In addition, the figure displays part of the *M. tuberculosis* trHbN specific tunnel/cavity system (grey mesh), proposed to support ligand diffusion to the heme. The black arrows underline the two entrance pathway of the molecular tunnel. The two observed conformations of PheE15 are also displayed (colored in red and gray). (B) Stereoview of the heme pocket region in cyano-met sperm whale Mb (PDB entry: 1EBC) (*13*, *62*), drawn in an orientation comparable to that of panel A; the protein backbone is drawn as red ribbons. Key interacting residues and the heme-Fe-bound cyanide are also displayed, together with the protein matrix sites identified in sperm whale Mb by binding of Xe atoms (numbered yellow spheres). Hydrogen bonds are represented by thin red lines in panel A and by a thin green line in panel B. α-Helical regions and key residues have been labeled according to the globin fold topology (*26*, *39*, *40*). Both pictures have been drawn with Molscript (*63*).

usually range between 1×10^2 and 1×10^3 M^{-1} s^{-1} (*1*−*15*).

The reaction of cyanide with ferrous Mbs and Hbs has received little attention due to the very low stability of the ensuing heme-Fe(II)-ligand complexes (the values of the association equilibrium constant are lower than 1×10^2 M^{-1}). Therefore, in most heme proteins, only values of the first-order ligand dissociation rate constant (i.e., k_{off}) have been determined, through experiments in which the ferrous cyanide complex is formed as a transient species following reduction of the ferric cyanide adduct. In turn, the transient heme-Fe(II)-cyanide complex dissociates into the reduced heme protein and HCN (*1*−*3*, *9*−*13*, *16*−*22*).

The reactivity of ferric and ferrous (non)vertebrate heme proteins toward cyanide is influenced mainly by the presence in the heme distal pocket of proton acceptor and donor group-(s), whose function is to assist the deprotonation of the incoming ligand and the protonation of the outgoing cyanide (*1*−*3*, *6*, *7*, *9*−*22*).

The present study reports both structural and functional aspects of cyanide binding to truncated hemoglobins (trHbs). TrHbs constitute a family of small oxygen-binding heme proteins distributed in eubacteria, cyanobacteria, protozoa, and plants, forming a distinct group within the Hb superfamily. Although trHbs are held to be of very ancient origin, none have been detected in the genomes of archaea or metazoa. TrHbs display amino acid sequences 20−40 residues shorter than (non)vertebrate Hbs and Mbs, to which they are scarcely related by sequence similarity. The trHb tertiary structure is based on a 2-on-2 α-helical sandwich, which represents a specific, and family conserved, editing of the well-known globin fold. The recent crystallographic analyses have identified an almost continuous hydrophobic tunnel, traversing the protein matrix, from the molecular surface to the heme distal site. Such a structural feature may provide a path for ligand diffusion to/from the heme (Figure 1) (*23*−*26*).

MATERIALS

Recombinant wild-type oxygenated *Mycobacterium tuberculosis* truncated hemoglobin-N (*M. tuberculosis* trHbN) was expressed and purified as described elsewhere (*27*). Recombinant wild-type oxygenated *M. tuberculosis* truncated hemoglobin-O (*M. tuberculosis* trHbO) was expressed and purified according to Mukai and co-workers (*28*). Recom-

Table 1: Data Collection and Crystallographic Refinement Statistics for the Cyanide Derivative of Ferric *M. tuberculosis* trHbN

resolution range (Å)	20−2.0
completeness (%)	99.5
R-merge (%)	13.7
unique reflections	17605
average $I/\sigma(I)$ (outer shell)	11 (4)
redundancy	4.2
no. of active protein and heme atoms	2056
no. of solvent, cyanide, and other nonprotein atoms	251
R-factor/*R*-free (%)[a]	17.8/23.5
rmsd from ideal geometry	
bond lengths (Å)	0.012
bond angles (°)	1.23
Ramachandran plot[b]	
most favored region (%)	97.2
additional allowed regions (%)	2.8
average *B*-factors (Å^2)	
main chain	23
side chain	24
solvent	33

[a] Calculated using 5% of the reflections. [b] Data produced with the program PROCHECK (*61*).

binant wild-type oxygenated *Chlamydomonas eugametos* truncated hemoglobin (*C. eugametos* trHb) was expressed as the sequence segment Ser22−Glu142, deleting the *N*-terminal chloroplast import sequence, and purified as reported elsewhere (*29*). The oxygenated heme protein concentration was determined using the following values of the molar absorptivity in the Soret region: *M. tuberculosis* trHbN, $\epsilon_{416\ nm} = 1.07 \times 10^5\ M^{-1}\ cm^{-1}$ (at pH 7.5, and 20.0 °C) (*27*); *M. tuberculosis* trHbO, $\epsilon_{414\ nm} = 1.13 \times 10^5\ M^{-1}\ cm^{-1}$ (at pH 7.5, and 23.0 °C) (*28*); and *C. eugametos* trHb, $\epsilon_{412\ nm} = 1.02 \times 10^5\ M^{-1}\ cm^{-1}$ (at pH 7.5, and 23.0 °C) (*29*). The HiTrap desalting column prepacked with Sephadex G-25 Superfine was provided by Amersham Pharmacia Biotech Italia (Cologno Monzese, MI, Italy). All the other products were from Merck AG (Darmstadt, Germany). All chemicals were of analytical or reagent grade and were used without further purification.

METHODS

Crystallographic Analysis of the Cyanide Derivative of Ferric M. tuberculosis trHbN. The cyanide derivative of ferric *M. tuberculosis* trHbN was crystallized by vapor diffusion against a 0.5-mL reservoir solution containing 2.25 M ammonium sulfate, 5.0×10^{-2} M phosphate buffer, pH 7.0. The 2 μL droplet contained 15 mg/mL protein, 1.0×10^{-3} M potassium cyanide, and 1.0×10^{-2} M potassium ferricyanide; the crystallization experiments were run at 4 °C.

Diffraction data were collected from one crystal (for cryoprotection, the crystal was soaked for about 20 s in a solution containing 20% (v/v) glycerol, 3.0 M ammonium sulfate, 1.0×10^{-3} M potassium cyanide, 5.0×10^{-2} M phosphate buffer, pH 7.0, before flash-freezing at 100 K in a liquid nitrogen stream) at the ESRF synchrotron source (Grenoble, France). Data were indexed and processed with the DENZO program suite (*30*). A total of 142 217 reflections were collected in the 20 to 2.0 Å resolution range, with an overall completeness of 99.5% (Table 1). The crystal belongs to the orthorhombic space group $P2_12_12_1$, with unit cell dimensions: $a = 44.57$ Å, $b = 61.44$ Å, $c = 91.29$ Å, two *M. tuberculosis* trHbN molecules per asymmetric unit.

To minimize any structural bias, the crystal structure of the cyanide derivative of ferric *M. tuberculosis* trHbN was solved by molecular replacement using the refined structure of *C. eugametos* trHb (40% identity) as search model (*23*), divided in eight zones (residues: 1−8, 9−24, 25−37, 38−52, 53−69, 80−97, 98−121, and heme), later refined as independent rigid bodies after the molecular replacement solution was found. The search model corresponded to 82% of the full molecule of the cyanide derivative of ferric *M. tuberculosis* trHbN, i.e., 49% of the scattering matter present in the asymmetric unit. The molecular replacement program EPMR (*31*) was employed, using data in the 15.0 to 4.0 Å resolution range. After locating the first molecule of the cyanide derivative of ferric *M. tuberculosis* trHbN in the asymmetric unit the correlation coefficient was 27.4%, *R*-factor = 58.5%. Location of the second independent molecule of the cyanide derivative of ferric *M. tuberculosis* trHbN brought the correlation coefficient to 47.5%, *R*-factor = 51.3%. Crystallographic refinement of the derived model allowed the building of the missing portions within the two molecules of the cyanide derivative of ferric *M. tuberculosis* trHbN, using the programs Refmac (version 5.29) (*32*), CNS (*33*), and O (*34*). The 2.0 Å resolution refined model contains 1970 protein atoms (residues 2−129 in each chain), 2 cyanide anions, 207 water molecules, and 6 sulfate ions (*R*-general = 17.8%, *R*-free = 23.5%) (Table 1), with close to ideal stereochemical parameters (*35*).

Cyanide Binding to Ferric trHbs. The ferric derivative of *M. tuberculosis* trHbN and trHbO as well as of *C. eugametos* trHb was prepared by oxidation of the oxygenated form with a 10-fold excess of potassium ferricyanide. After the reaction was allowed to proceed to completion, the protein was purified from ferri/ferrocyanide by desalting over a HiTrap desalting column prepacked with Sephadex G-25 Superfine equilibrated with 5.0×10^{-2} M phosphate buffer (pH 7.0) (*28*).

Kinetics for cyanide binding to ferric *M. tuberculosis* trHbN and trHbO as well as *C. eugametos* trHb was followed spectrophotometrically between 380 and 460 nm. Experiments were carried out by mixing the ferric trHb (i.e., trHb(III)) (final concentration, 2.0×10^{-6} to 5.0×10^{-6} M) with different amounts of cyanide (i.e., HCN; final concentration, 5.0×10^{-5} to 1.0×10^{-3} M).

Kinetics was analyzed within the framework of the minimum reaction mechanism 1 in which the dissociation rate of the ferric cyanide derivative of trHb (i.e., trHb(III)-CN^-) can be ignored due to its very low value in comparison to cyanide binding rate to ferric heme proteins (Scheme 1) (*1*).

Values of k_{on} for cyanide binding to ferric *M. tuberculosis* trHbN and trHbO as well as to ferric *C. eugametos* trHb have been determined from the linear dependence of the apparent combination first-order rate constant (i.e., k^{obs}) on the ligand concentration (i.e., [HCN]), under pseudo-first-order conditions (i.e., [HCN] > [trHb(III)]), according to eqs 1 and 2 (*1*):

$$[\text{trHb(III)CN}^-]_t = [\text{trHb(III)}]_i e^{-k_{obs}t} \quad (1)$$

$$k^{obs} = k_{on}[\text{HCN}] \quad (2)$$

The kinetic absorption spectra of the cyanide derivative of ferric *M. tuberculosis* trHbN and trHbO as well as of *C.*

Scheme 1

$$\text{trHb(III)} + \text{HCN} \xrightarrow{k_{on}} \text{trHb(III)-CN}^- + \text{H}^+$$

Scheme 2

$$\text{trHb(III)-CN}^- + \text{dithionite} \xrightarrow{h} \text{trHb(II)-CN}^- + \text{H}^+ \xrightarrow{k_{off}} \text{trHb(II)} + \text{HCN}$$

eugametos trHb were reconstructed from the static absorption spectra of trHb(III), plus the total optical density change at each wavelength measured in the rapid-mixing experiments. The static absorption spectra of trHb(III)-CN^- of *M. tuberculosis* trHbN and trHbO as well as of *C. eugametos* trHb were obtained by adding potassium cyanide (final concentration, 1.0×10^{-3} M) to the trHb(III) solution (final concentration, 5.0×10^{-6} M). All the experiments were carried out at pH 7.0 (1.0×10^{-1} M phosphate buffer) and 20.0 °C.

Transient Formation of trHb(II)-CN^- and Cyanide Dissociation. Kinetics of cyanide dissociation from ferrous *M. tuberculosis* trHbN and trHbO as well as *C. eugametos* trHb was measured by mixing the ferric trHb(III)-CN^- buffered solution (2.0×10^{-6} to 5.0×10^{-6} M trHb and 1.0×10^{-3} M cyanide) with a dithionite buffered solution (1.0×10^{-3} to 1.0×10^{-2} M). The cyanide concentration (1.0×10^{-3} M) exceeded the value of the dissociation equilibrium constant for cyanide binding to ferric globins (10^{-5}–10^{-6} M) (*1*, *3*, *9*), but was lower than that estimated for ligand saturation of the ferrous form ($<10^{-2}$ M) (*1*, *3*, *9*). The reaction was followed spectrophotometrically between 380 and 460 nm.

The time courses were fitted to two consecutive exponential processes according to the minimum reaction mechanism (Scheme 2) (*9*, *17*–*22*), where *h* is the rate constant (of order lower than two; see below) for the reduction of trHb(III)-CN^- by dithionite to the transient species trHb(II)-CN^-. Values of the dithionite-dependent apparent first-order rate constant for the reduction of trHb(III)-CN^- to transient trHb(II)-CN^- (h^{obs}) and of k_{off} have been determined from data analysis, according to eqs 3–5 treating both reactions as irreversible first-order processes (*36*):

$$[\text{trHb(III)-CN}^-]_t = [\text{trHb(III)-CN}^-]_i \times e^{-h_{obs}t} \quad (3)$$

$$[\text{trHb(II)-CN}^-]_t = [\text{trHb(III)-CN}^-]_i(h^{obs}((e^{-h_{obs}t}/(k_{off} - h^{obs})) + (e^{-k_{off}t}/(h^{obs} - k_{off})))) \quad (4)$$

$$[\text{trHb(II)}]_t = [\text{trHb(III)-CN}^-]_i - ([\text{trHb(III)-CN}^-]_t + [\text{trHb(II)-CN}^-]_t) \quad (5)$$

Since the trHb(III)-CN^- reducing species is SO_2^- (a dissociation product of dithionite) (*37*), the value of *h* has been determined from the linear dependence of h^{obs} on the square root of dithionite concentration (i.e., $[Na_2S_2O_4]^{1/2}$), under pseudo-first-order conditions (i.e., $[Na_2S_2O_4] > [\text{trHb(III)}]$), according to eq 6 (*18*):

$$h^{obs} = h[Na_2S_2O_4]^{1/2} \quad (6)$$

The kinetic absorption spectra of the transient species trHb(II)-CN^- and of the deoxygenated end-species trHb(II) were built from the static spectrum of trHb(III)-CN^- plus the calculated values of the optical density changes at each wavelength measured in the rapid-mixing experiments (see eqs 3–5). The static absorption spectra of the cyanide derivative of ferrous *M. tuberculosis* trHbN and trHbO as well as of ferrous *C. eugametos* trHb were obtained in the presence of 2.0 M potassium cyanide and 1.0×10^{-2} M sodium dithionite. The static absorption spectra of the deoxygenated derivative of ferrous *M. tuberculosis* trHbN and trHbO as well as of ferrous *C. eugametos* trHb were obtained in the presence of 1.0×10^{-2} M sodium dithionite. All the experiments were carried out at pH 7.0 (1.0×10^{-1} M phosphate buffer) and 20.0 °C.

RESULTS AND DISCUSSION

Three-Dimensional Structure of the Cyanide Derivative of Ferric M. tuberculosis trHbN. In the heme distal site of ferric *M. tuberculosis* trHbN the cyanide ligand is coordinated to the heme-Fe(III) atom, at 1.84 and 1.70 Å for subunits A/B, respectively, with an Fe−C−N angle of 171° (for both subunits). The heme-Fe(III) atom is contained in the heme plane (−0.03/−0.04 Å from the plane in subunits A/B, respectively), with a mean distance from the heme pyrrole N atoms of 2.03 and 2.04 Å in subunits A/B, respectively (Figure 1 and Table 2). The heme-Fe(III)-bound cyanide is stabilized by a tight hydrogen bond to the TyrB10(33) OH group (2.56/2.77 Å, in A/B subunits, respectively). The positioning of the TyrB10(33) side chain is dictated primarily by van der Waals contacts to neighboring residues, but also by a hydrogen bond to GlnE11(58) (3.02 Å, in both subunits). The latter residue, in turn, is at 3.47 Å from the heme-Fe(III)-bound cyanide in subunit A (3.41 Å in subunit B) (Figure 1). Thus, as previously observed for the heme-Fe(II)-bound O_2 in oxygenated trHbN (*24*), the cyanide ligand is stabilized by a network of distal site hydrogen bonds, which may compensate for the absence of a polar residue at the E7 site, where trHbN hosts LeuE7(54). Moreover, residues ThrCD4(49), ArgE6(53), LeuE7(54), and LysE10(57) face the heme distal cavity rendering the cyanide (or biatomic ligand, in general) binding site fully inaccessible to solvent through the so-called "E7 gate".

The analysis of the coordination distance for the heme-Fe(III)-CN^- bond in ferric *M. tuberculosis* trHbN is indicative of a tightly bound cyanide, likely representing a fully oxidized heme-Fe(III) atom, as opposed to selected cases reported in the literature for Hbs, Mbs, or unrelated heme proteins, for which heme-Fe(II) reduction occurs (at various levels) during X-ray irradiation of the crystalline samples (*13*). This finding might reflect the different mechanisms occurring in the Hbs or Mbs to achieve ligand stabilization in the heme distal cavity (*13*). On the proximal heme side, the HisF8(81)−Fe coordination bond is 2.11/1.99 Å (subunits A/B, respectively), and the proximal HisF8(81) azimuthal orientation is staggered relative to the heme pyrrole N-atoms (Figure 1 and Table 1), and almost unchanged relative to the oxygenated trHbN structure (*24*).

Such a binding mode of cyanide to ferric *M. tuberculosis* trHbN is reminiscent of the binding geometry observed for O_2 in oxygenated *M. tuberculosis* trHbN (*24*). However, the orientation of the anionic ligand in the ferric cyanide derivative of *M. tuberculosis* trHbN is almost perpendicular to the heme plane, whereas O_2 in oxygenated *M. tuberculosis*

Table 2: Heme-Fe(III) Atom and Cyanide Coordination Geometry Observed in the Cyanide Derivatives of Ferric *M. tuberculosis* trHbN and trHbO, as well as of Ferric *C. eugametos* trHb

	M. tuberculosis trHbN[a] (present study) PDB entry: 1RTE	*M. tuberculosis* trHbO[b] (*25*) PDB entry: 1NGH	*C. eugametos* trHb[c] (*23*) PDB entry: 1DLY	sperm whale Mb (*13*) PDB entry: 1EBC
resolution (Å)	2.0[e]	2.1	1.8	1.8
R-factor (%)	17.8[e]	18.6	17.6	18.1
average Fe−N (heme) distance (Å)	2.03/2.04[f]	2.04	1.98	2.03
Fe−HisF8 (NE2) distance (Å)	2.11/1.99[f]	2.05	2.18	2.02
Fe−CN (C) distance (Å)	1.84/1.70[f]	1.87/1.84[g]	2.65	2.02
Fe−CN (N) distance (Å)	3.01/2.87[f]	2.99/2.97[g]	3.48	3.06
C−N (CN) distance (Å)	1.17[e]	1.16	1.13	1.06
E7−CN (N) distance (Å)[d]	4.03/4.22[f]	6.00/6.81[g]	2.92	2.68
Fe−C−N angle (°)	171[e]	162/165[g]	130	166

[a] Values for the stereochemical parameters of the A and B independent subunits of *M. tuberculosis* trHbN are reported. [b] Average values for the 12 *M. tuberculosis* trHbO subunits hosted in the crystal asymmetric unit. [c] Owing to X-ray induced partial reduction of the heme Fe center, the cyanide coordination geometry reflects an average between a regularly Fe(III) coordinated ligand and a (Fe(II)) partly unbound species, trapped in the distal site cavity. The B-factors for cyanide C and N atoms are 15 and 21 Å^2, respectively (*23*). [d] Residue E7 is Leu in *M. tuberculosis* trHbN, Ala in *M. tuberculosis* trHbO, Gln in *C. eugametos* trHb, and His in sperm whale Mb (see text and Figure 1). [e] Data concerning A and B subunits are identical. [f] Data concerning A and B subunits, respectively. [g] Two distinct molecular populations, each composed of six subunits, can be distinguished in the trHbO dodecameric assembly (*25*).

trHbN displays a tilted orientation, with an Fe−O−O angle of about 118°, pointing toward the rear end of the heme crevice (*24*). Such an orientation is geometrically compatible with hydrogen bonds between both O atoms of the dioxygen molecule and the TyrB10(33) OH group (*24*).

TrHbO is an homologous *M. tuberculosis* protein belonging to a separate trHb group (19.7% sequence identity to trHbN) (*25*, *26*). Sequence analysis and the trHbO crystal structure have shown that the heme distal site is markedly affected by unusual residue substitutions relative to *M. tuberculosis* trHbN. In particular, trHbO displays a Tyr residue at the CD1(36) site, an Ala residue at the E7(44) site, whereas a Trp residue at site G8(88) (substituting for ValG8(94) in trHbN) protrudes into the distal site cavity, limiting its size. Moreover, half of the subunits in the crystallized dodecameric trHbO display a covalent link between TyrB10(23) and TyrCD1(36), expected to affect significantly the dynamical behavior of the heme distal site. The crystal structure of the cyanide derivative of ferric *M. tuberculosis* trHbO shows that the heme-Fe(III)-bound cyanide is roughly perpendicular to the heme plane (the average Fe−C−N angle is 164°), with an Fe-cyanide coordination distance ranging between 1.77 and 2.34 Å in the 12 subunits. The cyanide ion is stabilized by hydrogen bonds to TyrCD1(36) and to TrpG8(88) side chains (2.7 ± 0.1 and 3.2 ± 0.1 Å, respectively) (Table 2) (*25*).

In ferric *C. eugametos* trHb, the Fe−cyanide coordination bond distance is 2.01 Å, and the Fe−C−N angle is 130° (Table 2). The hydrogen bond distance between cyanide and the TyrB10(20) residue is 2.57 Å. Residues GlnE7(41) and GlnE11(45) may also provide cyanide stabilization through hydrogen bonds. However, the nature and cyanide stabilization capability of this hydrogen bond network may vary with the dynamics of the heme-distal site. The cyanide electron density and the observed coordination geometry (Table 2) suggest that the ligand may be present in more than one binding mode (*23*), reflecting X-ray-induced (partial) heme-Fe reduction (*13*).

Figure 1 shows the cyanide binding geometry to ferric sperm whale (*Physeter catodon*) Mb, generally taken as the prototype of monomeric oxygen carriers (*3*, *38*). The heme-Fe(III)-C(cyanide) coordination distance is 2.02 Å, and the Fe−C−N angle is 166°, the Fe atom being in plane with respect to the porphyrin pyrrole N atom (Table 2). Such a binding mode is indicative of a tightly bound cyanide to ferric sperm whale Mb, likely representing a fully oxidized heme-Fe(III) atom. The heme-Fe(III)-bound cyanide is in contact with PheCD1(43) (3.63 Å) and ValE11(68) (3.35 Å), essentially through the N atom, which in turn is hydrogen bonded to the heme distal HisE7(64) NE2 atom (2.68 Å). Note that the HisE7(64) residue locks the heme-Fe(III)-bound cyanide in the heme distal site and makes it fully inaccessible to solvent (*13*).

Cyanide Binding to Ferric trHbs. Values of k^{obs} for cyanide binding to ferric *M. tuberculosis* trHbN and trHbO as well as *C. eugametos* trHb conform to a single-exponential decay and are independent of the observation wavelength, at fixed HCN concentration. Note that cyanide binding to both monomeric and multimeric ferric heme proteins follows monophasic kinetics, indicating that the quaternary state does not affect ligand binding (*1*−*7*, *9*−*11*, *13*−*15*). Unusually, *Vitreoscilla* sp. homodimeric ferric Hb has been reported to display anticooperative cyanide binding properties (*12*).

Values of k_{on} for cyanide binding to ferric heme proteins (Table 3) are essentially unaffected by the heme-Fe(III) geometry. In fact, sperm whale Mb, horse heart Mb, *Parascaris equorum* Hb, *Scapharca inaequivalvis* HbI, human Hb, and trout HbI and HbIV bind a water molecule at the sixth coordination position of the heme-Fe(III) atom, around neutrality (*9*, *39*−*44*). On the other hand, *C. eugametos* trHbN is in the low-spin hexacoordinate form, between pH 7 and 8 (*29*). By contrast, *M. tuberculosis* trHbN and trHbO, *Aplysia limacina* Mb, and *Glycera dibranchiata* monomeric Hb (component C) are high-spin pentacoordinate systems, around neutrality (*27*, *28*, *43*, *45*−*47*).

The reactivity of cyanide toward ferric heme proteins has been postulated to be influenced mainly by the presence in the heme pocket of proton acceptor group(s), whose function is to assist the deprotonation of the incoming ligand (i.e., HCN). This interpretation is in agreement with (i) the very slow kinetics of cyanide binding to *Glycera dibranchiata* monomeric Hb (component C; $k_{on} = 4.9 \times 10^{-1}$ M^{-1} s^{-1}; pH 7.0 and 20.0 °C) (see Table 3 for comparison), which lacks both the heme-Fe(III)-bound water molecule and the

Table 3: Values of Kinetic Parameters for Cyanide Binding to and Dissociation from (Non)Vertebrate Globins as Well as for the Reduction of Heme-Fe(III)-cyanide Complexes

(non)vertebrate globin	k_{on} (M^{-1} s^{-1})	h ($M^{-1/2}$ s^{-1})	k_{off} (s^{-1})
C. eugametos trHb[a]	4.6×10^2	3.5	1.6×10^{-2}
M. tuberculosis trHbN[a]	3.8×10^2	3.1	1.2×10^{-2}
M. tuberculosis trHbO[a]	3.2×10^2	2.8	1.3×10^{-2}
A. limacina Mb	2.0×10^{2b}	$\geq 1 \times 10^{2c}$	2.2×10^{-2c}
sperm whale Mb	1.4×10^{2b}	4.4[c]	2.1×10^{-2c}
horse heart Mb	1.7×10^{2d}	8.0×10^{1e}	1.5×10^{-1e}
P. equorum Hb	n.d.[l]	8.0×10^{-2f}	1.1×10^{-2f}
S. inaequivalvis HbI[g]	2.3×10^2	0.60	1.9×10^{-2}
human Hb tetramer	1.1×10^{2h}	2.0×10^{-1i}	1.2×10^{-1} (R-state)[i] 1.5 (T-state)[i]
human Hb α-chain	1.7×10^{2j}	2.0×10^{-2i}	1.7×10^{-1i}
human Hb β-chain	1.6×10^{2j}	1.8[i]	1.5×10^{-1i}
trout Hb I tetramer	n.d.	5.3×10^{1k}	5.65[k]
trout Hb IV tetramer	n.d.	5.4×10^{1k}	6.0[k] 5.5×10^{-1k}

[a] pH 7.0, 20.0 °C. Present study. [b] pH 7.0, 20.0 °C. From ref *8*. [c] pH 7.0, 20.0 °C. Recalculated from ref *19*. [d] pH 7.0, 22.0 °C. From ref *1*. [e] pH 8.2, 25.0 °C. Recalculated from ref *18*. [f] pH 7.1, 20.0 °C. Recalculated from ref *21*. [g] pH 9.2, 20.0 °C. From ref *9*. [h] pH 6.05, 20.0 °C. From ref *4*. [i] pH 7.0, 20.0 °C. From ref *20*. [j] pH 7.0, 20.0 °C. From ref *4*. [k] pH 7.2, 20.0 °C. From ref *22*. [l] n.d., not determined.

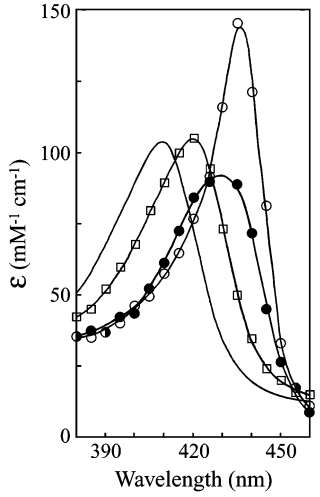

FIGURE 2: Static and kinetic absorption spectra (lines and symbols, respectively) in the Soret region of ferric and ferrous derivatives of *M. tuberculosis* trHbO. trHb(III), continuous line; trHb(III)-CN^-, continuous line and squares; trHb(II)-CN^-, continuous line and open circles; and trHb(II), continuous line and filled circles. The kinetic spectra of trHb(III)-CN^- (squares), trHb(II)-CN^- (circles), and trHb-(II) (filled circles) were reconstructed from the static absorption spectra of trHb(III) or trHb(III)-CN^- plus the total optical density change at each wavelength measured in the rapid-mixing experiments. Values of λ_{max} (nm) and ϵ (mM^{-1} cm^{-1}) of the absorption spectra in the Soret region of ferric and ferrous derivatives of *M. tuberculosis* trHbO are shown in Table 4. Absorption spectra were obtained at pH 7.0 (0.1 M phosphate buffer) and 20.0 °C. For further experimental details, see text.

residue(s) catalyzing proton exchange, and (ii) the effect of changes in the polarity of the heme distal pocket of human Mb, pig Mb, and sperm whale Mb by site-directed mutagenesis (*3*, *6*, *7*).

As shown in Figure 2, the static and kinetic absorption spectra of the cyanide derivative of ferric *M. tuberculosis* trHbO are in excellent agreement. This occurs also for *M. tuberculosis* trHbN and *C. eugametos* trHb (data not shown), excluding the occurrence of detectable intermediates in the

Table 4: Values of λ_{Max} and ϵ of the Absorption Spectra in the Soret Region of Some Derivatives of Ferric and Ferrous *M. tuberculosis* trHbN and trHbO as well as of *C. eugametos* trHb[a]

heme protein	trHb(III)	trHb(III)-CN^-	trHb(II)-CN^-	trHb(II)
M. tuberculosis trHbN	*406*[b]	*418*	*435*	*432*
	141[b]	**102**	**142**	**103**
M. tuberculosis trHbO	*409*[c]	*419*	*436*	*429*
	104[c]	**105**	**144**	**92**
C. eugametos trHb	*409*[d]	*416*	*434*	*426*
	114[d]	**97.6**	**149**	**108**

[a] Values of λ_{max} (nm) are in italic; values of ϵ (mM^{-1} cm^{-1}) are in bold. All absorption spectra were obtained at pH 7.0 (1.0×10^{-1} M phosphate buffer) and 20.0 °C. [b] High spin hexacoordinate heme. From ref *27*. [c] High spin hexacoordinate heme. From ref *28*. [d] Low-spin hexacoordinate heme. From ref *29*.

cyanide binding reaction. Values of λ_{max} and ϵ of the absorption spectra in the Soret region of the cyanide derivative of ferric *M. tuberculosis* trHbN and trHbO as well as *C. eugametos* trHb are given in Table 4. Around neutrality, the ferric derivative of *M. tuberculosis* trHbN and trHbO is a high-spin hexacoordinate species (*27*, *28*), the ferric derivative of *C. eugametos* trHb being a low-spin hexacoordinate species (*29*) (Table 4). The absorption spectra of the cyanide derivative of ferric *M. tuberculosis* trHbN and trHbO as well as *C. eugametos* trHb in the Soret region (Table 4) are similar to those reported for (non)vertebrate heme proteins (*1*−*15*), despite the different residues building up the heme distal pocket (*3*, *13*, *23*−*25*, *27*−*29*, *39*−*41*, *45*−*51*).

Transient Formation of trHb(II)CN^- and Cyanide Dissociation. The overall reaction of the cyanide derivative of ferric *M. tuberculosis* trHbN and trHbO as well as of *C. eugametos* trHb (i.e., trHb-Fe(III)-CN^-) with dithionite conforms to the minimum two-step sequential reaction Scheme 2 (Figure 3, panel A), in good agreement with previous results (*9*, *17*−*22*). The first reaction is the reduction of trHb-Fe(III)-CN^- to trHb-Fe(II)-CN^- driven by dithionite. In agreement with Lambeth and Palmer (*37*), SO_2^- (a dissociation product of $Na_2S_2O_4$) is the reducing species, as demonstrated by the linear dependence of the apparent reduction first-order rate constant h^{obs} on the square root of $Na_2S_2O_4$ concentration (Figure 3B). The second reaction conforms to a irreversible monomolecular decay (Figure 3A) of the trHb-Fe(II)-CN^- reaction intermediate into trHb-Fe-(II) and HCN. Under all the experimental conditions, cyanide dissociation from trHb-Fe(II)-CN^- is much slower than the reduction of the heme-Fe(III) atom (Table 3).

Simultaneous fit of the experimental data at each wavelength to Scheme 2 shows that the intermediate trHb-Fe(II)-CN^- is a unique and well-identified species and allowed calculation of the fully populated trHb-Fe(II)-CN^- and of trHb(II) absorption spectra (Figure 2). The intermediate and final spectroscopic species given in Scheme 2 correspond to trHb-Fe(II)-CN^- and trHb-Fe(II), respectively, on the basis of the following experimental evidence: (i) the $Na_2S_2O_4$ concentration dependence of the rate constant h^{obs} for the buildup of the intermediate (Figure 3A,B); (ii) the simple irreversible monomolecular decay of trHb-Fe(II)-CN^- into trHb-Fe(II) and HCN (Figure 3A); and (iii) the excellent agreement between the static and kinetic absorption spectra

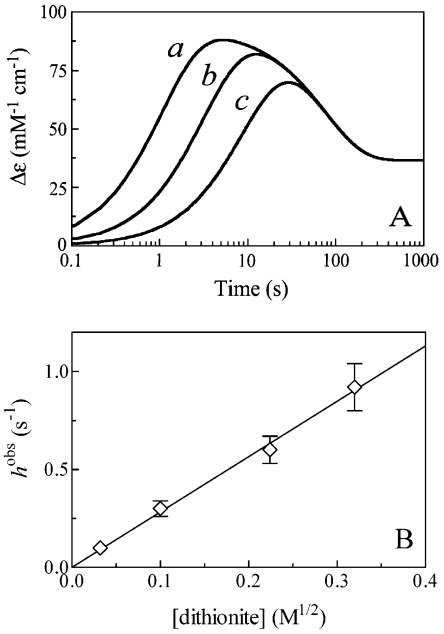

FIGURE 3: Kinetics for the dithionite-dependent reduction of the cyanide derivative of ferric *M. tuberculosis* trHbO and for cyanide dissociation from the ferrous species. (A) Time course of trHb-(III)-CN^- reduction and cyanide dissociation. The dithionite concentration was 1.0×10^{-1} M (trace a), 1.0×10^{-2} M (trace b), and 1.0×10^{-3} M (trace c). The cyanide concentration was 1.0×10^{-3} M. The ferric *M. tuberculosis* trHbN concentration was 5.0×10^{-6} M. The continuous lines were calculated according to eqs 3−5 (*36*) with the following values of h^{obs}: 9.2×10^{-1} s^{-1} (trace a), 3.1×10^{-1} s^{-1} (trace b), 1.0×10^{-1} s^{-1}, and (trace c); and the dithionite concentration-independent value of $k_{off} = 1.3 \times 10^{-2}$ s^{-1}. (B) Dependence of the pseudo first-order rate constant h^{obs} for the reduction of trHb(III)-CN^- on the dithionite concentration. The continuous line was calculated according to eq 6 (*18*) with $h = 2.8$ M$^{-1/2}$ s^{-1}. All data were obtained at pH 7.0 (0.1 M phosphate buffer) and 20.0 °C. For further experimental details, see text.

of trHb-Fe(II)-CN^- and trHb-Fe(II) (Figure 2). The excellent agreement between the static and kinetic absorption spectra of trHb-Fe(II)-CN^- and trHb-Fe(II) (Figure 2) excludes the occurrence of further detectable intermediates in the cyanide dissociation process from trHb-Fe(III)-CN^- via the transient formation of trHb-Fe(II)-CN^-. Values of λ_{max} and ϵ of the absorption spectra in the Soret region of the deoxygenated and ferrous cyanide derivatives of *M. tuberculosis* trHbN and trHbO as well as of *C. eugametos* trHb are given in Table 4. The absorption spectra of trHb-Fe(II)-CN^- and trHb-Fe(II) are similar to those reported for (non)vertebrate globins (*9*, *17*−*22*), despite the different heme-distal residues (*9*, *17*−*25*, *27*−*29*, *39*−*41*, *45*−*51*).

Values of h for the reduction of the cyanide derivative of ferrous heme proteins range between 2.0×10^{-2} M$^{-1/2}$ and $\geq 1 \times 10^{2}$ M$^{-1/2}$ s^{-1} (Table 3), possibly reflecting the different ability of (non)vertebrate globins considered to bind dithionite or its dissociation product SO_2^-. Note that dithionite binding to human deoxygenated Hb occurs at the interface of two tetramers in the crystal lattice by hydrogen bonds or salt interactions with HisG16(116) and HisG17(117) of the β_2 subunit and LysA13(16) of the α_1 subunit of the adjacent Hb molecule (*52*). Indeed, electron transfer within a protein matrix should occur in the millisecond time range (*53*), not limiting the reaction investigated here.

Values of k_{off} for cyanide dissociation from both monomeric and multimeric heme proteins range between 1.1×10^{-2} and 6.0 s^{-1} (Table 3), possibly reflecting the different nature and geometry of the heme distal residue(s) hydrogen bonded to the heme-bound cyanide (Figure 1) (*23*−*25*, *27*−*29*, *39*−*41*, *45*, *46*, *48*−*51*) which would assist protonation of the outgoing cyanide (*9*, *17*−*22*). Unusually, biphasic kinetics indicates subunit heterogeneity in cyanide dissociation from ferrous tetrameric trout HbIV (*22*). On the other hand, cyanide cooperative dissociation from ferrous human Hb has been reported, values of k_{off} reflecting the quaternary state (i.e., the R- or T-form) of the tetramer, as observed for oxygen, carbon monoxide, nitric oxide, and isocyanides (*20*).

Interestingly, *G. dibranchiata* monomeric Hb (component C) displays very fast kinetics for both dithionite-induced reduction and cyanide dissociation. In fact, upon mixing the Hb-Fe(III)-CN^- complex with dithionite, the deoxygenated ferrous derivative (i.e., Hb-Fe(II)) is obtained within 10 ms, without detection of the Hb-Fe(II)-CN^- intermediate (*19*).

CONCLUSIONS

Ligand diffusion to the trHb heme distal site is a peculiar case, since the access to the distal cavity through the so-called "E7 gate", at least in group N trHbs, is prevented. To compensate this, *M. tuberculosis* trHbN and *C. eugametos* trHb display a protein matrix tunnel/cavity system, of apolar nature, which connects the solvent space to the heme distal site. A less continuous, but topologically equivalent, system of inner cavities is present in *M. tuberculosis* trHbO, where the small size of the distal AlaE7(44) residue may allow ligand diffusion through the "E7 gate" (*23*−*26*).

Within the N and O trHb groups (*26*), O_2, NO, and CO all combine with the ferrous deoxygenated derivative at similar rates. These ligand-independent combination rates indicate that the electronic factors that give rise to the large ligand-specific differences in most (non)vertebrate Mbs and Hbs are not operative in trHbs. In fact, ligand binding to trHbs appears to be limited by intraprotein ligand diffusion (*54*). However, similar ligand entry rate values have been reported for *M. tuberculosis* trHbN and sperm whale Mb ($\approx 2 \times 10^7$ M^{-1} s^{-1}). On the other hand, the ligand entry rate for *M. tuberculosis* trHbO ranges between 1×10^5 and 1×10^6 M^{-1} s^{-1} (*54*, *55*). Preliminary molecular dynamics simulation experiments on O_2 diffusion in *M. tuberculosis* trHbN indicate that, once the ligand enters the tunnel/cavity system, it can diffuse to the heme distal site within 400 ps.[2]

Mechanisms involving ligand accumulation in the trHb matrix should be also considered (*56*). In fact, the trHb tunnel/cavity systems (Figure 1) can accommodate as many as six CO molecules, as judged from volume analysis and kinetic experiments (*56*). A similar situation may hold also for cyanide accumulation in trHb's since cyanide is isosteric and isoelectronic with CO (*2*). Moreover, at least four Xe atoms are present in the tunnel/cavity system of *M. tuberculosis* trHbN crystals, following treatment at 25 bar Xe pressure.[2] Similar experimental procedures have shown that sperm whale Mb may trap a maximum of two ligand molecules in the protein matrix at Xe1 and Xe4 sites (Figure 1) (*55*, *57*, *58*).

Despite the observed structural differences, values of the second-order kinetic rate constant for cyanide binding to

[2] M. Milani, personal communication.

ferric (non)vertebrate globins (characterized by the so-called "E7 gate", such as *A. limacina Mb* and sperm whale Mb) (*59*, *60*), and to trHbs (characterized by the protein matrix tunnel/cavity system) (*23*−*26*) are similar and quite low (Table 3). Such an observation suggests that cyanide binding is primarily unaffected by the protein structural properties defining the overall diffusion mechanism to the heme distal pocket. Indeed, kinetics of cyanide binding have been shown to be primarily and comparably limited in ferric (non)-vertebrate globins by proton transfer to the solvent (*3*, *6*, *7*), despite the involvement of entirely different cyanide-heme-distal residue(s) (e.g., His, Tyr, and/or Gln) hydrogen bond networks (Figure 1) (*3*, *13*, *23*−*25*, *27*−*29*, *39*−*41*, *45*−*51*).

The rate constants for the reduction of the heme-Fe(III)-cyanide complexes here considered, on the contrary, span 4 orders of magnitude (Table 3). This may reflect the different ability of (non)vertebrate globins considered to yield productive complex(es) with dithionite, or with its byproduct SO_2^- (*18*). As reported for the cyanide derivative of ferric (non)-vertebrate globins (*3*, *6*, *7*), values of the rate constant for ligand dissociation from heme-Fe(II)-cyanide of (non)-vertebrate heme proteins are very different (Table 3), possibly reflecting the nature and stereochemistry of the heme distal residue(s) assisting protonation of the outgoing cyanide (*9*, *17*−*22*). However, values of the rate constant for heme-Fe(II)-cyanide dissociation in trHbs and in sperm whale Mb are similar (Table 3), possibly reflecting a striking case of convergent evolution.

ACKNOWLEDGMENT

We wish to thank Mr. Angelo Merante for graphical assistance.

REFERENCES

1. Antonini, E., and Brunori, M. (1971) *Hemoglobin and Myoglobin in their Reactions with Ligands*, North-Holland Publishing Co., Amsterdam.
2. Brunori, M., Coletta, M., Ascenzi, P., and Bolognesi, M. (1989) Kinetic control of ligand binding processes in hemoproteins. *J. Mol. Liq. 42*, 175−193.
3. Bolognesi, M., Bordo, D., Rizzi, M., Tarricone, C., and Ascenzi, P. (1997) Nonvertebrate hemoglobins: structural bases for reactivity. *Prog. Biophys. Mol. Biol. 68*, 29−68.
4. Gibson, Q. H., Parkhurst, L. J., and Geraci, G. (1969) The reaction of methemoglobin with some ligands. *J. Biol. Chem. 244*, 4668−4676.
5. Job, D., Zeba, B., Puppo, A., and Rigaud, J. (1980) Kinetic studies of the reaction of ferric soybean leghemoglobins with hydrogen peroxide, cyanide and nicotinic acid. *Eur. J. Biochem. 107*, 491−500.
6. Mintorovitch, J., van Pelt, D., and Satterlee, J. D. (1989) Kinetic study of the slow cyanide binding to *Glycera dibranchiata* monomer hemoglobin components III and IV. *Biochemistry 28*, 6099−6104.
7. Brancaccio, A., Cutruzzolà, F., Travaglini Allocatelli, C., Brunori, M., Smerdon, S. J., Wilkinson, A. J., Dou, Y., Keenan, D., Ikeda-Saito, M., Brantley, R. E., Jr., and Olson, J. S. (1994) Structural factors governing azide and cyanide binding to mammalian metmyoglobins. *J. Biol. Chem. 269*, 13843−13853.
8. Nardini, M., Tarricone, C., Rizzi, M., Lania, A., Desideri, A., De Sanctis, G., Coletta, M., Petruzzelli, R., Ascenzi, P., Coda, A., and Bolognesi, M. (1995) Reptile heme protein structure: X-ray crystallographic study of the aquo-met and cyano-met derivatives of the loggerhead sea turtle (*Caretta caretta*) myoglobin at 2.0 Å resolution. *J. Mol. Biol. 247*, 459−465.
9. Boffi, A., Ilari, A., Spagnuolo, C., and Chiancone, E. (1996) Unusual affinity of cyanide for ferrous and ferric *Scapharca inaequivalvis* homodimeric hemoglobin: equilibria and kinetics of the reaction. *Biochemistry 35*, 8068−8074.
10. Boffi, A., Chiancone, E., Takahashi, S., and Rousseau, D. L. (1997) Stereochemistry of the Fe(II)- and Fe(III)-cyanide complexes of the homodimeric *Scapharca inaequivalvis* hemoglobin. A resonance Raman and FTIR study. *Biochemistry 36*, 4505−4509.
11. Boffi, A., Chiancone, E., Peterson, E. S., Wang, J., Rousseau, D. L., and Friedman, J. M. (1997) Dynamics of cyanide binding to ferrous *Scapharca inaequivalvis* homodimeric hemoglobin. *Biochemistry 36*, 4510−4514.
12. Bolognesi, M., Boffi, A., Coletta, M., Mozzarelli, A., Pesce, A., Tarricone, C., and Ascenzi, P. (1999) Anticooperative ligand binding properties of recombinant ferric *Vitreoscilla* homodimeric hemoglobin: a thermodynamic, kinetic and X-ray crystallographic study. *J. Mol. Biol. 291*, 637−650.
13. Bolognesi, M., Rosano, C., Losso, R., Borassi, A., Rizzi, M., Wittenberg, J. B., Boffi, A., and Ascenzi, P. (1999) Cyanide binding to *Lucina pectinata* hemoglobin I and to sperm whale myoglobin: a X-ray crystallographic study. *Biophys. J. 77*, 1093−1099.
14. Ilari, A., Bonamore, A., Farina, A., Johnson, K. A., and Boffi, A. (2002) The X-ray structure of ferric *Escherichia coli* flavohemoglobin reveals an unexpected geometry of the distal heme pocket. *J. Biol. Chem. 277*, 23725−23732.
15. Park, H. J., Yang, C., Treff, N., Satterlee, J. D., and Kang, C. (2002) Crystal structures of unligated and CN-ligated *Glycera dibranchiata* monomer ferric hemoglobin components III and IV. *Proteins 49*, 49−60.
16. Keilin, D., and Hartree, E. F. (1955) Cyanide compounds of ferroperoxidase and myoglobin and their reversible photodissociation. *Biochem. J. 61*, 153−171.
17. Cox, R. P., and Hollaway, M. R. (1977) The reduction by dithionite of Fe(III) myoglobin derivatives with different ligands attached to the iron atom: a study by rapid-wavelength-scanning stopped-flow spectrophotometry. *Eur. J. Biochem. 74*, 575−587.
18. Olivas, E., De Waal, D. J., and Wilkins, R. G. (1977) Reduction of metmyoglobin derivatives by dithionite ion. *J. Biol. Chem. 252*, 4038−4042.
19. Bellelli, A., Antonini, G., Brunori, M., Springer, B. A., and Sligar, S. G. (1990) Transient spectroscopy of the reaction of cyanide with ferrous myoglobin: effect of distal side residues. *J. Biol. Chem. 265*, 18898−18901.
20. Brunori, M., Antonini, G., Castagnola, M., and Bellelli, A. (1992) Cooperative cyanide dissociation from ferrous hemoglobin. *J. Biol. Chem. 267*, 2258−2263.
21. Antonini, G., Bellelli, A., Concetti, A., Falcioni, G., and Brunori, M. (1994) Cyanide dissociation from the hemoglobin of *Parascaris equorum*. *Biochim. Biophys. Acta 1025*, 252−257.
22. Antonini, G., Bellelli, A., Brunori, M., and Falcioni, G. (1996) Kinetic and spectroscopic properties of the cyanide complexes of ferrous haemoglobins I and IV from trout blood. *Biochem. J. 314*, 533−540.
23. Pesce, A., Couture, M., Dewilde, S., Guertin, M., Yamauchi, K., Ascenzi, P., Moens, L., and Bolognesi, M. (2000) A novel two-over-two alpha-helical sandwich fold is characteristic of the truncated hemoglobin family. *EMBO J. 19*, 2424−2434.
24. Milani, M., Pesce, A., Ouellet, Y., Ascenzi, P., Guertin, M., and Bolognesi, M. (2001) *Mycobacterium tuberculosis* hemoglobin N displays a protein tunnel suited for O_2 diffusion to the heme. *EMBO J. 20*, 3902−3909.
25. Milani, M., Savard, P. Y., Ouellet, H., Ascenzi, P., Guertin, M., and Bolognesi, M. (2003) A TyrCD1/TrpG8 hydrogen bond network and a TyrB10TyrCD1 covalent link shape the heme distal site of *Mycobacterium tuberculosis* hemoglobin O. *Proc. Natl. Acad. Sci. U.S.A. 100*, 5766−5771.
26. Wittenberg, J. B., Bolognesi, M., Wittenberg, B. A., and Guertin, M. (2002) Truncated hemoglobins: a new family of hemoglobins widely distributed in bacteria, unicellular eukaryotes, and plants. *J. Biol. Chem. 277*, 871−874.
27. Couture, M., Yeh, S., Wittenberg, B. A., Wittenberg, J. B., Ouellet, Y., Rousseau, D. L., and Guertin, M. (1999) A cooperative oxygen-binding hemoglobin from *Mycobacterium tuberculosis*. *Proc. Natl. Acad. Sci U.S.A. 96*, 11223−11228.
28. Mukai, M., Savard, P. Y., Ouellet, H., Guertin, M., and Yeh, S. R. (2002) Unique ligand-protein interactions in a new truncated hemoglobin from *Mycobacterium tuberculosis*. *Biochemistry 41*, 3897−3905.
29. Couture, M., and Guertin, M. (1996) Purification and spectroscopic characterization of a recombinant chloroplastic hemoglobin from

the green unicellular alga *Chlamydomonas eugametos*. *Eur. J. Biochem. 242*, 779−787.
30. Otwinoski, Z., and Minor, W. (1997) Processing of X-ray diffraction data collected in oscillation mode. *Methods Enzymol. 276*, 307−326.
31. Kissinger, C. R., Gehlhaar, D. K., and Fogel, D. B. (1999) Rapid automated molecular replacement by evolutionary search. *Acta Crystallogr., Sect. D: Biol. Crystallogr. 55*, 484−491.
32. Murshudov, G. N., Vagin, A. A., and Dodson, E. J. (1997) Refinement of macromolecular structures by the maximum-likelihood method. *Acta Crystallogr., Sect. D: Biol. Crystallogr. 53*, 240−255.
33. Brünger, A. T., Adams, P. D., Clore, G. M., Delano, W. L., Gros, P., Grosse-Kunstleve, R. W., Jiang, J.-S., Kuszewski, J., Nilges, M., Pannu, N. S., Read, R. J., Rice, L. M., Simonson, T., and Warren, G. L. (1998) Crystallography and NMR System: a new software suite for macromolecular structure determination. *Acta Crystallogr., Sect. D: Biol. Crystallogr. 54*, 905−921.
34. Jones, T. A., Zou, J. Y., Cowan, S. W., and Kjeldgaard, M. (1991) Improved methods for building protein models in electron density maps and the location of errors in these models. *Acta Crystallogr., Sect. A: Found. Crystallogr. 47*, 110−119.
35. Engh, R. A., and Huber, R. (1991) Accurate bond and angle parameters for X-ray protein structure refinement. *Acta Crystallogr., Sect. A: Found. Crystallogr. 47*, 392−400.
36. Bateman, H. (1910) Solution of a system of differential equations occurring in the theory of radio-active transformations. *Proc. Cambridge Phyl. Soc. 15*, 423−427.
37. Lambeth, D. O., and Palmer, G. (1973) The kinetics and mechanism of reduction of electron-transfer proteins and other compounds of biological interest by dithionite. *J. Biol. Chem. 248*, 6095−6103.
38. Frauenfelder, H., McMahon, B. H., and Fenimore, P. W. (2003) Myoglobin: the hydrogen atom of biology and a paradigm of complexity. *Proc. Natl. Acad. Sci. U.S.A. 100*, 8615−8617.
39. Takano, T. (1977) Structure of myoglobin refined at 2.0 Å resolution: I. crystallographic refinement of metmyoglobin from sperm whale. *J. Mol. Biol. 110*, 537−568.
40. Perutz, M. F. (1979) Regulation of oxygen affinity of hemoglobin: influence of structure of the globin on the heme iron. *Annu. Rev. Biochem. 48*, 327−386.
41. Aime, S., Fasano, M., Paoletti, S., Arnelli, A., and Ascenzi, P. (1995) NMR relaxometric investigation on human methemoglobin and fluoromethemoglobin: an improved quantitative in vitro assay of human methemoglobin. *Magn. Res. Med. 33*, 827−831.
42. Falcioni, G., Fortuna, G., Giardina, B., Brunori, M., and Wyman, J. (1977) Functional properties of partially oxidized trout hemoglobins. *Biochim. Biophys. Acta 490*, 171−177.
43. Giacometti, G. M., Ascenzi, P., Brunori, M., Rigatti, G., Giacometti, G., and Bolognesi, M. (1981) Absence of water at the sixth coordination site in ferric *Aplysia* myoglobin. *J. Mol. Biol. 151*, 315−319.
44. Coletta, M., Falcioni, G., Concetti, A., Ascoli, F., and Brunori, M. (1986) Ligand-dependent behavior of the hemoglobin from the ascarid *Parascaris equorum*. *Biochim. Biophys. Acta 870*, 169−175.
45. Bolognesi, M., Onesti, S., Gatti, G., Coda, A., Ascenzi, P., and Brunori, M. (1989) *Aplysia limacina* myoglobin: crystallographic analysis at 1.6 Å resolution. *J. Mol. Biol. 205*, 529−544.
46. Conti, E., Moser, C., Rizzi, M., Mattevi, A., Lionetti, C., Coda, A., Ascenzi, P., Brunori, M., and Bolognesi, M. (1993) X-ray crystal structure of ferric *Aplysia limacina* myoglobin in different liganded states. *J. Mol. Biol. 233*, 498−508.
47. Padlan, E. A., and Love, W. (1974) Three-dimensional structure of hemoglobin from the polychaete annelid, *Glycera dibranchiata*, at 2.5 Å resolution. *J. Biol. Chem. 249*, 4067−4078.
48. Royer, W. E. Jr. (1994) High-resolution crystallographic analysis of a co-operative dimeric hemoglobin. *J. Mol. Biol. 235*, 657−681.
49. Yang, J., Kloek, A. P., Goldberg, D. E., and Matthews, F. S. (1995) The structure of *Ascaris* hemoglobin domain I at 2.2 Å resolution: molecular features of oxygen avidity. *Proc. Natl. Acad. Sci. U.S.A. 92*, 4224−4228.
50. Tame, J. R., Wilson, J. C., and Weber, R. E. (1996) The crystal structures of trout Hb I in the deoxy and carbonmonoxy forms. *J. Mol. Biol. 259*, 749−760.
51. Xia, Z., Zhang, W., Nguyen, B. D., La Mar, G. N., Kloek, A. P., and Goldberg, D. E. (1999) ^{1}H NMR investigation of the distal hydrogen bonding network and ligand tilt in the cyanomet complex of oxygen-avid *Ascaris suum* hemoglobin. *J. Biol. Chem. 274*, 31819−31826.
52. Wireko, F. C., and Abraham, D. J. (1992) The crystal state binding of dithionite to deoxy-hemoglobin. *Protein Eng. 5*, 3−5.
53. Gray, H. B., and Winkler, J. R. (1996) Electron transfer in proteins. *Annu. Rev. Biochem. 65*, 537−561.
54. Ouellet, H., Juszczak, L., Dantsker, D., Samuni, U., Ouellet, Y. H., Savard, P. Y., Wittenberg, J. B., Wittenberg, B. A., Friedman, J. M., and Guertin, M. (2003) Reactions of *Mycobacterium tuberculosis* truncated hemoglobin O with ligands reveal a novel ligand-inclusive hydrogen bond network. *Biochemistry 42*, 5764−5774.
55. Scott, E. E., Gibson, Q. H., and Olson, J. S. (2001) Mapping the pathways for O_2 entry into and exit from myoglobin. *J. Biol. Chem. 276*, 5177−5188.
56. Samuni, U., Dantsker, D., Ray, A., Wittenberg, J. B., Wittenberg, B. A., Dewilde, S., Moens, L., Ouellet, Y., Guertin, M., and Friedman, J. M. (2003) Kinetic modulation in carbonmonoxy derivatives of truncated hemoglobins: the role of distal heme pocket residues and extended apolar tunnel. *J. Biol. Chem. 278*, 27241−27250.
57. Scott, E. E., and Gibson, Q. H. (1997) Ligand migration in sperm whale myoglobin. *Biochemistry 36*, 11909−11917.
58. Teeter, M. M. (2004) Myoglobin cavities provide interior ligand pathway. *Protein Sci. 13*, 313−318.
59. Bolognesi, M., Cannillo, E., Ascenzi, P., Giacometti, G. M., Merli, A., and Brunori, M. (1982) Reactivity of ferric *Aplysia* and sperm whale myoglobins towards imidazole. X-ray and binding study. *J. Mol. Biol. 158*, 305−315.
60. Perutz, M. F. (1989) Myoglobin and haemoglobin: role of distal residues in reactions with haem ligands. *Trends Biochem. Sci. 14*, 42−44.
61. Laskowski, R. A., MacArthur, M. W., Moss, D. S., and Thornton, J. M. (1993) PROCHECK, a program to check the stereochemical quality of protein structures. *J. Appl. Crystallogr. 26*, 283−291.
62. Tilton, R. F., Jr., Kuntz, I. D., Jr., and Petsko, G. A. (1984) Cavities in proteins: structure of a metmyoglobin-xenon complex solved to 1.9 Å. *Biochemistry 23*, 2849−2857.
63. Kraulis, P. J. (1991) MOLSCRIPT: a program to produce both detailed and schematic plots of protein structures. *J. Appl. Crystallogr. 24*, 946−950.

BI049870+